HHS Public Access

Author manuscript

Biomed Pharmacother. Author manuscript; available in PMC 2023 May 04.

Published in final edited form as:

Biomed Pharmacother. 2023 May ; 161: 114554. doi:10.1016/j.biopha.2023.114554.

Piperlongumine inhibits proliferation and oncogenic MYCN expression in chemoresistant metastatic retinoblastoma cells directly and through extracellular vesicles

Cui Shi[a,b], **Kunhui Huang**[a,b], **John Soto**[a], **Renuka Sankaran**[a,b], **Vrinda Kalia**[c], **Onyekwere Onwumere**[a,d], **Michael Young**[e], **Linda Einbond**[a], **Stephen Redenti**[a,b,d,*]

[a]Lehman College, the City University of New York, 250 Bedford Park Boulevard West, Bronx, NY 10468, USA

[b]Biochemistry Doctoral Program, The Graduate School, City University of New York, 365 Fifth Avenue, New York, NY 10016, USA

[c]Department of Environmental Health Sciences, Columbia University Mailman School of Public Health, New York, NY 10032, USA

[d]Biology Doctoral Program, The Graduate School of the City University of New York, 365 5th Avenue, New York, NY 10016, USA

[e]The Schepens Eye Research Institute, Massachusetts Eye and Ear, Harvard Medical School, 20 Staniford Street, Boston, MA 02114, USA

Abstract

Ocular retinoblastoma malignancies, which develop into metastatic phenotypes, result in poor prognosis and survival for infant and child patients. To improve the prognosis of metastatic retinoblastoma, it is important to identify novel compounds with less toxic side effects and higher therapeutic efficacy compared to existing chemotherapeutics. Piperlongumine (PL), a neuroprotective, plant-derived compound has been explored for its anticancer activities both in vitro and *in vivo*. Here, we analyze the potential efficacy of PL for metastatic retinoblastoma cell treatment. Our data reveal that PL treatment significantly inhibits cell proliferation in metastatic retinoblastoma Y79 cells compared to the commonly used retinoblastoma chemotherapeutic drugs carboplatin, etoposide, and vincristine. PL treatment also significantly increases cell death compared to treatment with other chemotherapeutic drugs. PL-induced cell-death signaling was

*Corresponding author at: Lehman College, the City University of New York, 250 Bedford Park Boulevard West, Bronx, NY 10468, USA. Stephen.Redenti@lehman.cuny.edu (S. Redenti).

CRediT authorship contribution statement

Cui Shi, Kunhui Huang, John Soto, Renuka Sankaran, Stephen Redenti: Conceptualization, Data curation, Formal analysis. **Linda Einbond, Onyekwere Onwumere, Vrinda Kalia, Michael Young, Renuka Sankaran**: Scientific design guidance, Manuscript review, Editing. **Cui Shi, Kunhui Huang, Renuka Sankaran, Stephen Redenti**: Writing − original draft, Figure, Data table generation. **Stephen Redenti**: Funding acquisition, Investigation, Methodology, Project administration.

Appendix A. Supporting information

Supplementary data associated with this article can be found in the online version at doi:10.1016/j.biopha.2023.114554.

Conflict of interest statement

The authors declare that there are no conflicts of interest.

associated with significantly higher caspase 3/7 activities and greater loss of mitochondrial membrane potential. PL was also internalized into Y79 cells with an estimated concentration of 0.310pM and expression analysis revealed reduced MYCN oncogene levels. We next examined extracellular vesicles derived from PL-treated Y79 cells. Extracellular vesicles in other cancers are pro-oncogenic, mediating systemic toxicities via the encapsulation of chemotherapeutic drugs. Within metastatic Y79 EV samples, an estimated PL concentration of 0.026pM was detected. PL treatment significantly downregulated Y79 EV cargo of the oncogene *MYCN* transcript. Interestingly, non-PL-treated Y79 cells incubated with EVs from PL-treated cells exhibited significantly reduced cell growth. These findings indicate that in metastatic Y79 cells, PL exhibits potent anti-proliferation effects and oncogene downregulation. Importantly, PL is also incorporated into extracellular vesicles released from treated metastatic cells with measurable anti-cancer effects on target cells at a distance from the site of primary treatment. The use of PL in the treatment of metastatic retinoblastoma may reduce primary tumor proliferation and inhibit metastatic cancer activity systemically via extracellular vesicle circulation.

Keywords

Metastatic retinoblastoma; Piperlongumine; Extracellular vesicles; Chemotherapeutic drugs; Chemoresistance; MYCN

1. Introduction

Retinoblastoma (RB) is the most common intraocular pediatric cancer and affects approximately 300 children annually in the United States [1]. With early detection in high-income countries, more than 90% of children with RB survive for more than five years, with a rate of recurrence from 6% to 45% [2]. In developing countries due to poor detection and treatment of primary retinoblastoma, [3], there is a 30–70% mortality rate [4]. Current treatments for RB include enucleation surgery, chemotherapy, laser or freezing, and radiation therapy. However, some of these treatments are associated with delayed growth, facial deformity, reduced vision, and kidney dysfunction [5]. In addition, a disease with a metastatic phenotype has a very poor prognosis, perhaps because the malignant tumor cells disseminate during the early stages of tumor formation [6]. Most metastatic RB patients will die approximately six months after diagnosis [7] and the frequency of this highly malignant phenotype ranges from 4.8% to 11% [8,9]. RB metastasis is a major contributor to mortality and is associated with poor life-long prognosis [8,10–13]. In addition, the long-term survivors of RB face life-long risks of developing secondary cancers, disease relapse, and severe late toxicity directly related to chemotherapeutic drugs.

Chemotherapy-induced toxicities and adverse effects, reported in other cancers, also occur in childhood patients treated for RB [14]. An important area of research is the identification of novel agents that can reduce RB malignancy with lower toxicities and greater therapeutic efficacy. Importantly, RB expresses intrinsic chemoresistant proteins which limit current chemotherapeutic approaches [15]. To this end, several studies have shown that naturally occurring plant compounds, including polyphenols and flavonolignans, reverse chemoresistance caused by repeated exposure to chemotherapeutic drugs [16] and

inhibit tumor cell dissemination [17]. Critical analysis of the effects of natural products on tumorigenicity in pediatric cancers, arising in the CNS and characterized by amplified oncogenes (e.g. MYCN Proto-Oncogene, BHLH Transcription Factor (MYCN)) needs to be performed.

In concert with cellular RB studies of the effects of natural products, RB-released extracellular vesicles (EVs) also require analysis to determine their significance in RB metastatic processes [18]. Chemotherapy-related systemic toxicities leading to poor prognosis and development of secondary tumors are mediated by EVs derived from both chemo-naïve and chemo-exposed primary tumor cells [19]. EVs are a heterogeneous population of lipid-enclosed particles of endocytic origin containing a range of molecular cargo including DNA, RNA, and protein [20]. Although EVs are known to harbor pro-oncogenic cargo [21], this is more pronounced in EVs derived from chemo-exposed tumor cells [22]. EVs are known to elevate the aggressive phenotypes of tumor cells [21], including promoting chemoresistance [23], and disease metastasis [24]. Therefore, it is essential to develop strategies to reduce the pro-oncogenicity of RB EVs.

In this work, we investigated the potential of piperlongumine (PL), a biologically active amide alkaloid extracted from the medicinal long pepper [25,26], to alter the pro-tumorigenic characteristics of cells and EVs in metastatic RB. PL is a small electrophilic molecule that has been shown to target and inhibit multiple cancer mechanisms including cell cycle and invasive metastatic machinery [27–29]. PL selectively kills cancer cells [29,30] by the generation of reactive oxygen species [31] associated with protein cross-linking, cell cycle arrest, and autophagy.

Data from this work reveal that PL elicits greater cytotoxic responses compared to current metastatic RB drugs including carboplatin (CBP), etoposide (ETOP), and vincristine (VINC), at comparable doses, suggesting a potential of PL for RB therapy. Treatment of Y79 cells with EVs released from PL-treated Y79 cells (PL-Y79-EVs) resulted in reduced cell viability. Quantitative polymerase chain reaction (qPCR) showed downregulation of *MYCN* transcripts in treated cells and PL-Y79-EVs. As MYCN proteins are considered a major driver for retinoblastoma [32], and they have been considered undruggable because of their chemical structure [33], we performed molecular docking of PL on Aurora A kinase, which is a crucial regulator of MYCN degradation [34]. Docking results showed that PL aligned very well with ATP at Aurora A ATP-binding pocket and partly disrupted its native conformation, leading to the degradation of MYCN protein. HPLC analyses of PL-Y79-EVs showed the presence of PL. The data suggest that PL functions as an inhibitor of RB tumorigenicity and metastatic processes by reducing RB cancer cell viability, inhibiting the cell cycle, and down-regulating MYCN. Importantly, encapsulation and transfer of PL in extracellular vesicles provide a mechanism for targeting both RB cells and other pre-cancerous cells at a distance, potentially inhibiting pro-oncogenic processes, metastasis, and RB recurrence (Graphical Abstract).

2. Methods

2.1. PL preparation

Drugs were purchased from Cayman Chemicals (Ann Arbor, MI, USA) and dissolved in dimethyl sulfoxide (DMSO; Sigma-Aldrich, St. Louis, MO, USA) to prepare a 10-mM stock, which was aliquoted and stored at − 20 °C until use. All working stocks of each drug were prepared to a final concentration of 0.01% DMSO.

2.2. Cell line and cell culture

The Y79 cell line was purchased from American Type Culture Collection (ATCC). Cells were maintained in RPMI-1640 media, supplemented with 20% fetal bovine serum (FBS) and 1% Penicillin-Streptomycin. Cells were grown in suspension and sub-cultured every 3–4 days as cultures reached 80% confluence. All cells were maintained in a humid environment with 5% CO2 at 37 °C. For EV experiments, cells were cultured in a like manner but with exosome-depleted serum. For the Y79 3D cell culture, cells were grown in Corning® Spheroid Microplates (Corning, NY, USA) to induce spheroid formation. Y79 cells were placed one cell per well in 100ul culture medina in a 96 well with Ultra-Low Attachment surface round bottom following the manufacturer's instruction. Cells were cultured for 6 days to allow the spheroid to form and ready for 3D cell viability assay.

2.3. Cell proliferation assay

2D Cell growth was assessed with WST-1 cell proliferation assay (Roche, Branchburg, NJ, USA), according to the manufacturer's instructions and as described by Gharbaran et al. [35]. One hundred microliters of medium-containing cells at 1×10^5 cells/ml were seeded in a 96-well plate and incubated overnight. The cells were then treated with 0, 5, and 10 μM of either dimethyl sulfoxide (DMSO), piperlongumine (PL), carboplatin (CBP), etoposide (ETOP), or vincristine (VINC) for 48 h in triplicates. For EV treatment analysis, untreated Y79 cells were incubated overnight with 8 ug EVs from PL-treated Y79 cells for 48 h in triplicates. Treated cells were then incubated with 10 μl WST-1 reagent for 3 h following standard cell culture conditions. Absorbance was read at 450 nm on a Synergy H1 Hybrid microplate reader (BioTek Instruments, Winooski, VT, USA). Cell growth (as a percentage) was computed as a ratio of the absorbance (A450) of treated (either drug or DMSO) cells to the absorbance of the untreated (0 μM) control. The assay principle is based on the conversion of the tetrazolium salt WST-1 into a colored dye by mitochondrial dehydrogenase enzymes. Y79 spheroid viability was assessed with CellTiter-Glo 3D Cell Viability Assay. Y79 cells were seeded one cell/well in 100ul media and cultured for 6 days. Cells were then treated with chemotherapy drugs and PL the same as WST-1 assay. After 48hrs, 100ul of CellTiter-Glo 3D Reagent was added to each well and the contents were mixed vigorously for 5 min to induce cell lysis. The plate was incubated at room temperature for an additional 25 min and luminescence was measured using the Synergy H1 Hybrid microplate reader.

2.4. Acridine orange and ethidium bromide live/dead assay

Acridine orange (AO)-ethidium bromide (EtBr)—AO/EtBr–assay was used to determine cell death as described by Gharbaran et al. (2020) [36]. One hundred μl of 1×10^5 cells/ml were seeded in 96-well plates overnight and then treated with 10 μM of each drug or vehicle (DMSO), for 48 h. Four μl of a solution consisting of 10 μg/ml each of AO and EtBr were added to each well of treated cells and immediately imaged. In this assay, the membrane-permeable AO stained live cells green, and EtBr, which is membrane-impermeable, stained the nuclei of dead cells orange to red.

2.5. Detection of mitochondrial membrane potential (Ψm)

Changes in Ψm were assessed by staining treated cells with JC-10 dye according to the manufacturer's (Sigma-Aldrich) instructions with modifications as described by Gharbaran et al. [35]. Five hundred microliters of medium containing cells at 2×10^5 cells/ml were seeded in poly-L-lysine (Sigma-Aldrich)-coated 20-mm microwells of 35 mm petri dish (MatTek Corporation, Ashland, MA, USA) overnight and then treated with the indicated doses of each compound or DSMA, for 48 h. The cells were then incubated in JC-10 Dye Loading Solution for 30 min following standard cell culture conditions. An aliquot (250 μl) of the JC-10 Dye Loading Solution-medium mix was withdrawn and replaced with 250 μl Assay Buffer B. Cells were immediately imaged.

2.6. Detection of caspase activities

Caspase 3/7 activities were analyzed using CellEvent Caspase-3/7 Green Detection Reagent (Life Technologies, CA, USA), according to the manufacturer's instructions and as described by Gharbaran et al. (2021) [35]. Cells were seeded and treated as described for the JC-10 Ψ_M assay. Cells were then incubated with CellEvent Caspase-3/7 Green Detection Reagent at a final concentration of 4 μM for 30 min, following standard cell culture conditions.

2.7. EV isolation and analysis

EVs were isolated from Y79 cells simultaneously plated and treated with 5 μM PL for 48 hrs. Cell culture condition media was collected and centrifuged at 800 g for 5 min to remove cells. The supernatant was then centrifuged at 12,000 g for 25 min at 4 °C. EVs were then pelleted by ultracentrifugation at 100,000 g for 70 min at 4 °C. The pellet was resuspended in 100ul of phosphate buffer saline (PBS). A sample of the EVs was analyzed for distribution of particle size on a ViewSizer 3000 (Horiba Ltd, Kyoto, Japan) according to the manufacturer's instructions and as described by Comfort et al. [37]. In this approach, the instrument tracks the particle by using three laser light sources with wavelengths of 450 nm, 520 nm, and 635 nm and recording particles simultaneously in multiple spectral bands. The EV samples were diluted at 1:500 with filtered PBS. Thirty videos (30 fps, 300 frames per video) were recorded at 22℃ with the following recording parameters: blue laser, 210 mW; green laser, 12 mW; red laser, 8 mW; exposure, 15 ms; camera gain, 30 dB. To get the accurate size distribution and particle concentration, the sample was automatically stirred to mix for 5 s between each recording. The particle counts and integrates into the range

from 50 to 1000 nm. The sample was calculated by accounting for the dilution factor and processed with the Main Chart in “LogBinSilica”.

2.8. RNA isolation, cDNA, and qPCR

RNA isolation, cDNA synthesis, and qPCR were performed as described by Gharbaran et al. [38], using Y79 cells treated with 10 μM PL and their EVs and untreated control Y79 cells and their EVs. Total RNA was isolated by Trizol (Life Technologies, Carlsbad; CA, USA, cat. # 155960218) according to manufacturer instructions. cDNA was prepared by ProtoScript® II First Strand cDNA Synthesis Kit (New England BioLabs, Rowley; MA, USA, cat. #: E6300S) according to the manufacturer’s instructions, from 50 ng of RNA per reaction. For qPCR, each reaction consisted of 10 ng cDNA, 10 mM primers, and 10 μl 2X SYBR GreenER™ qPCR SuperMix (Life Technologies, cat. #: 11761–100). Reactions were carried out in a MicroAmp Fast Optical 96-Well Reaction Plate on a BioRad Icycler Thermal Cycler. The reaction was performed using the standard mode (initial denaturation at 95 °C for 10 min followed by 40 cycles of 95 °C for 15 s and 60 °C for 1 min). Each qPCR reaction was done in triplicate. The amount of target mRNA was normalized to the expression levels of the housekeeping gene GAPDH. Primers pairs for the genes were GAPDH forward 5′-TGCACCACCAACTGCTTAGC-3′ and reverse 5′- GGCATGGACTG TGGTCATGAG-3′; MYCN forward 5′- CACAAGGCCCTCAGTACCTC − 3′ and reverse 5′-ACCACGTCGATTTCTTCCT-3′; KIF14 forward 5′-GCAC TTTCGGAACA AGCAAACCA-3′ and reverse 5′-ATGTTGCTGGCAGC GGGACTAA-3′; E2F3 forward 5′-GATGATGTAACAGCCCCAAGGA-3′ and reverse 5′-TGCG GTGTAAGAGAGCCCTTT-3′; MDM4 forward 5′-GGGAAGGATCAACACCAGAAAC AACC-3′ and reverse 5′-CAATC CCAAAGACAGACCCATAGGC − 3′. The ΔΔCt method was used to calculate the fold-change relative to controls.

2.9. Extraction of PL-treated or untreated cell and EV metabolomics

All the samples are mixed with 1.5 ml of 100% LC-MS grade methanol (Sigma-Aldrich Co. LLC) and incubated in-− 80 ℃ for 30 mins. The sample/methanol mixture is vortexed for 5 mins and sonicated for 10 mins in a 0℃ water bath. The mixtures were centrifuged at 14,000 g for 10 min at 4 ℃. The pellet from the separation was re-extracted by the same procedure and the combined metabolite-containing supernatants were evaporated to dryness under nitrogen gas for the UPLC-MS analysis. All the procedures were performed on dry ice to avoid heating the sample.

2.10. Molecular docking of PL on MYCN regulator Aurora A kinase

The molecular docking process was performed by OpenEye scientific application (OpenEye Scientific Software, Inc., Santa Fe, NM, USA; https://www.eyesopen.com). The Aurora-A MYCN complex (PDB entry: 7ZTL[39]) was a query from the RCSB protein data bank(https://www.rcsb.org/) and prepared by the SPRUCE module of OpenEye applications in default parameters. The co-crystalized bonded ligand ADP (ADP 501) was used to identify the binding site during the protein preparation. The 3D conformers of ligand ADP and PL were generated by the OEOmege module (classic model). The 200 conformers of each ligand then were docked to the prepared binding site of Aurora-A N-MYC complex using the FRED module (default settings) of OEDocking. The resulting files were saved

with the best pose of both ligands, ADP and PL, in mol2 format and edited with Chimera (Chimera 1.16, UCSF) [40].

2.11. High-resolution liquid chromatography-mass spectrometry of cell and EV extracts

Standard stock solutions of PL were dissolved in DMSO at 1 mg/ml and 0.1 mg/ml. Working standard solutions were prepared from the stock solution of PL by diluting with acetonitrile. All the solutions were stored at − 20 °C. Extracts were analyzed by high-resolution liquid chromatography-mass spectrometry (LCMS). LCMS was performed on an Agilent 6550 iFunnel Q-TOF mass spectrometer coupled to an Agilent 1290 Infinity LC system (binary pump, diode array detector, and autosampler). Chromatography was performed using an Agilent SB-C8 column (2.1 ×50 mm) at 45 °C and a gradient of solvents A (water, 0.1% formic acid) and B (acetonitrile, 0.1% formic acid) from 2% to 98% solvent B in 10 min at a flow rate of 0.2 ml/min. The following settings were applied to the ESI source: gas temperature, 250 °C; nebulizer, 30 PSIG; sheath gas temperature, 250 °C; Vcap, 3500 V; and nozzle voltage, 2000 V. For MS analysis, full scan mass spectra (m/z = 100–3000) were acquired in positive-ion mode. Data were acquired and analyzed using Agilent's MassHunter Software suite (Data Acquisition B.09.00, Qualitative Analysis B.07.00). Dried cell extracts were resuspended in acetonitrile (100 μl) and 5 μl injections were analyzed. For the piperlongumine (PL) standard, 1 μl of a 1 pM concentration was analyzed. Concentration estimates for cell and EV extracts were determined by using the extracted ion chromatograms (EIC) peak integrations for both the $[M+H]^+$ and $[M+Na]^+$ ions ($C_{17}H_{19}NO_5$). EIC peak areas of putative isomers were summed and compared to the peak area of a single PL (1 pM) standard.

2.12. Microscopy

Images of stained cells were captured with a CoolSNAP HQ2 CCD camera (Cool SNAP EZ, Photometrics, Tucson, AZ, USA) coupled to a Nikon Ti Eclipse inverted microscope (Melville, NY, USA).

2.13. Statistical analyses

Data analyses were performed using SAS 9.1.4 (Cary, NC, USA) and StatView 5 (Cary, NC, USA). Analysis of variance (One-way ANOVA) and F statistics were used to determine significant differences between the means as defined by $p < 0.05$. Data obtained from the assays on WST-1 cell proliferation, AO/EtBr, and caspase3/7 staining are presented as plus or minus standard error of the mean (± SEM). Cell count data was generated from at least five microscopic fields per dose of each compound. For the cell growth assay, the mean per dose was determined from triplicates. Each experiment was repeated at least three times. For ratio analysis, n = 5 experimental samples per condition were compared to the control to determine significance using unpaired t-tests, data is plotted ± SEM.

3. Results

3.1. PL is more potently inhibitory to the growth of RB cells than chemotherapy drugs

Studies show that PL potently induces anti-tumor activities at relatively low doses [27,41]. Because PL is neuroprotective [42] and produces anti-inflammatory responses [43], it

is likely to produce fewer toxic effects in vivo, compared to chemotherapeutic drugs. Therefore, we compared the PL-induced growth responses of Y79 cells to those of the chemotherapeutic drugs CBP, ETOP, and VINC that are currently being used in RB clinical trials. Y79 cells incubated overnight were treated for 48 h with indicated doses (0, 5, and 10 μM) of either dimethyl sulfoxide (DMSO), PL, CBP, ETOP, or VINC (Fig. 1A). Cell growth was assessed using a WST-1 proliferation assay. The results showed that PL induces a significant decrease in cell growth in a dose-dependent manner compared to CBP, ETOP, and VINC ($p < 0.05$) (Fig. 1B). Phase contrast microscopic images also showed that Y79 cells treated with PL (10 μM) resulted visually in greater loss of membrane integrity compared to other drugs at the same dose (Fig. 1C). This result was also confirmed in a Y79 3D spheroid culture model. The CellTiter-Glo 3D reagent penetrates spheroids and measures ATP which is detected as a luminescent signal and indicator of a number of viable cells. Spheroids treated with PL showed significantly decreased ATP levels compared to treatments with CBP, ETOP, and VINC. This data demonstrates that PLs anticancer activity observed in 2D retinoblastoma culture is retained and extends its potency to multicellular 3D retinoblastoma spheroids.

3.2. PL induces significantly greater cell death

We next compared the cell death responses between PL and the chemotherapeutic drugs. To do this, Y79 cells treated with 0, 5, and 10 μM of each compound for 48 h, were analyzed using acridine-orange (AO)/Ethidium bromide (EtBr) −AO/EtBr− live/dead staining. Live cells stain green with AO and dead cells emit red-orange fluorescence with EtBr (Fig. 2A) Qualitative analysis showed that the PL treatment resulted in a larger percentage of EtBr-positive (EtBr+) Y79 cells compared to cells treated with drugs. Analyses by one-way ANOVA of cell count data, obtained from microscopic images, showed that PL treatment resulted in significantly higher levels of cell death compared to chemotherapeutic drugs (CBP, ETOP, or VINC) (One-way ANOVA, $p < 0.05$)(Fig. 2B).

3.3. PL induces greater loss of mitochondrial potential in Y79 cells

A feature of apoptotic cell death is the disruption of mitochondrial function including changes in the mitochondrial membrane potential ($\Delta \Psi_M$), which is an indicator of mitochondrial health and oxidation-reduction state [44]. To determine the effects of PL on mitochondrial function, $\Delta \Psi_M$ was assessed after 48 h of treatment. JC-10, a cationic dye that accumulates potential-dependently in mitochondria, was used to measure changes in Ψ_M. With this dye, the loss of Ψ_M is followed by a red-to-green shift, indicating a loss of Ψ_M in low-viability cells. Cells with active mitochondria show red fluorescence. In our experiments, under the same concentration (10 μM), Y79 cells treated with chemotherapeutic drugs CBP, ETOP, or VINC maintain more red aggregates which were either absent from or decreased in cells treated with PL (10 μM) for 48 h (Fig. 3), indicating that PL induces greater loss of Ψ_M of Y79 cells.

3.4. PL induces significantly higher caspase3/7 activities in Y79 cells

Activation of the caspase cascade is an indicator of programmed cell death [45]. Members of the caspase family, including caspase3/7, are activated in response to chemotherapeutic drugs [46]. To determine whether PL induces cell death via caspase3/7 activation, Y79 cells

were treated for 48 h with PL and stained with a caspase3/7-specific fluorochrome dye (Fig. 4A). The results show that the PL-treated group expresses significantly more casp3/7 + than either CBP, ETOP, or VINC-treated Y79 cells. Analysis of microscopic images of cells stained with the casp3/7 dye showed that PL induced a significantly higher proportion of casp3/7 + activities in Y79 cells compared to CBP, ETOP, or VINC (One-way ANOVA, $p < 0.05$) (Fig. 4B).

3.5. PL modifies the oncogenic signaling of RB extracellular vesicles

Because tumor-derived EVs encapsulate cargo that facilitates cancer development, metastasis, and chemoresistance [23,24], we next focused on the potential of PL to alter Y79-derived EV properties. Y79 EVs were isolated from control and experimental culture media at 48 hrs. Nanoparticle tracking analysis (NTA) was performed using the ViewSizer 3000 to determine average diameters and release concentration (Fig. 6A, B). Y79 EV average diameter for control was 148 nm + /− 59 nm with a concentration of 1.1E+ 11 particles/ml. PL-treated experimental Y79-EVs exhibited an average diameter of 164 nm + /− 68 nm at a concentration of 1.3E+ 11 particles/ml. To determine whether PL alters the oncogenic cargo of Y79-EVs, Y79 cells were treated with PL for 48 hrs and EVs were analyzed for the presence and potential changes in oncogenes including MDM4 Regulator Of P53 (MDM4), Kinesin Family Member 14 (KIF14), E2F transcription factor 3 (E2F3) and MYCN. KIF14 and E2F3 are predicted to facilitate proliferation and are overexpressed in RB [47]. MDM4 and MYCN are reported to be involved in the pro-oncogenic signaling of RB [48]. PL-treated cells showed a trend of decreased levels of MYCN compared to the control (Fig. 5C). Importantly, PL significantly reduced the levels of MYCN in EVs (Fig. 5C). While the gene transcripts for KIF14, E2F3, and MDM4 were detected across EV conditions, expression levels did not exhibit significant differences (Fig. S1). Multiple oncogenes present in retinoblastoma EVs may facilitate pathogenic processes including tumor growth, metastasis, and resistance to therapy [49]. Next, effects of EVs from PL-treated Y79 cells (PL-Y79-EVs) on target Y79 cells. The viability of Y79 cells co-incubated with PL-Y79-EVs had significantly reduced cell growth (Fig. 5D). These results indicate that PL reduces the oncogenic cargo of metastatic Y79 EVs with the potential to exert similar effects via EV signaling at a distance.

3.6. UPLC-MS analysis for PL encapsulated in EVs

Emerging studies suggest that EVs can be carriers for natural products, including those with anti-oncogenic properties [50]. Therefore, to further characterize PL Y79-EV cargo and assess whether the induced decrease in target cell viability may be due to their encapsulation and transfer of PL, we compared the metabolomic contents of PL-Y79-EVs to control EVs, using Ultra-high Performance Liquid Chromatography-MS (UPLC-MS). UPLC-MS/MS has high sensitivity and selectivity for the detection and identification of chemical compounds. Both the PL-treated Y79 cells (Fig. 6 A1) and PL-Y79-EVs (Fig. 6 B1) exhibit peaks at the same retention time, which are absent in the control untreated Y79 cells (Fig. 6A2) and corresponding control EVs (Fig. 6B2). The chromatogram of the PL standard shows the peak at the retention time of 5.86 (Fig. 6A3, B3). A second peak is also present in the cell samples which may be a PL metabolite resulting from cellular metabolism. The data suggest that PL is encapsulated by the PL-treated Y79 cells and their released EVs. The peak area of

extracted samples and the PL standards are used to calculate the estimated concentration of PL. An estimated PL concentration of 0.309598 pM was detected in treated Y79 cells and a concentration of 0.026462 pM in their released EVs. The estimated PL concentration here is derived from a small percentage of the total EVs isolated.

3.7. PL predicted inhibition of Aurora A kinase leading to degradation of MYCN

As PL downregulated MYCN in this work and MYCN overexpression is associated with retinoblastoma pathogenesis [51] we next investigated mechanisms of PL regulation of MYCN using molecular docking analysis. MYCN protein has been considered undruggable due to its chemical structure having no active site for small compound binding. But its degradation is highly regulated by Aurora A kinase, and disruption of the Aurora A/MYCN complex will cause loss of MYCN [34] (Fig. 7). Several ATP-competitive inhibitors of Aurora A at the ATP binding pocket have been identified to potently bind Aurora A at its inactivation conformation and disrupt the Aurora-A/MYCN complex, leading to the degradation of MYCN. We performed molecular docking of PL on Aurora A kinase and tested its alignment with ADP at the binding pocket. The docking result showed that PL aligned very well and shared similar protein-ligand interaction with ADP. The PL can form H-bonds with the Aurora protein at residue LYS162 and LYS143 (Fig. 7) that were consistent with ADP to Aurora A protein. This indicated that PL has the potential to disrupt the ATP binding of Aurora A, which is essential to the protection of MYCN from being phosphorylated and degraded.

4. Discussion

In the current study, we assessed the potential of PL as a candidate molecule for metastatic RB therapy. Our approach involves comparing the cytotoxic responses of RB cells and spheroids to PL and selected chemotherapeutic compounds (CBP, ETOP, and VINC) and analyzing PLs reduction of pro-oncogenic properties of metastatic RB EVs. The underlying rationale for this approach is based on reports that common therapeutic drugs enhance cancer metastasis, chemoresistance, and malignant phenotypes mediated by EVs [19,24]. CBP enters cells via passive diffusion and transporters, its mechanism of action is binding to DNA and inhibiting transcription which leads to cell death [52,53]. VINC uptake by has been described as carrier-mediated transport and its mechanism of action is microtubule depolymerization leading to cell-cycle arrest [54,55]. VINC has been studied in combination with other therapeutic drugs for RB treatment in clinical trials [56,57] and has been associated with colorectal cancer and neurotoxicity [58,59]. ETOP diffuses across the cell membrane and functions by inhibiting topoisomerase II, leading to DNA damage and apoptotic cell death [60, 61]. In this study, the results showed that at comparable doses, PL exerts greater growth-limiting effects than either CBP, ETOP, or VINC. Staining of the treated cells with AO/EtBr solution revealed a statistically greater proportion of cell death caused by PL than by either CBP, ETOP, or VINC. Assaying for changes in $\Delta\Psi M$ with JC-10 dye revealed qualitatively greater loss of $\Delta\Psi M$ in PL-treated cells than in cells treated with either CBP, ETOP, or VINC. Additionally, treatment of cells with PL resulted in greater levels of caspase 3/7 activation compared to the chemotherapeutic drugs. Finally, the results

showed that PL downregulates the *MYCN* transcripts carried in metastatic RB-derived EVs, and Y79 cells treated with these EVs showed decreased cell growth.

In our study, the doses (0, 5, and 10 μM) at which PL induces growth-limiting and cytotoxic effects are consistent with those of other studies including RB and other cancer types [30,62,63]. The dose at which PL exerts these effects in our study is much lower than the range of doses displayed by chemotherapeutic drugs. Zhu et al. (2021) showed a dose-dependent decrease in the viability of wild-type Y79 cells treated with 0–200 μM CBP (IC50 ~ 40 μM at 24 h) [64]. However, doses of CBP, ETOP, and VINC ranging from 50 μ to 200 μM are required to produce similar levels of cell viability [64] reported for 5–10 μM of PL in our study. These observations suggest that PL is likely to exert greater anti-cancer potential compared to chemotherapeutic drugs in vitro. The relatively low dose-high cytotoxic effects of PL in our study are likely a consequence of the selective targeting of the aberrant oncogenic pathways, ROS pathways, and transcription factors in Y79 cells. For example, PL inhibits the growth of Y79 cells by induction of apoptosis but this was associated with the downregulation of FOXM1[62]. On the other hand, most chemotherapeutic drugs, including those used in standard RB treatment regimens (CBP, ETOP, and VINC), are non-selective and therefore, may require either longer treatment time or higher doses to elicit cytotoxic responses.

We also reported that PL-induced growth inhibition of Y79 cells is in part due to cell death. In general, programmed cell death is regulated by two apoptotic pathways: the death receptor-dependent extrinsic pathway and a mitochondrial-dependent intrinsic pathway [65]. mitochondrial-dependent apoptosis involves disruption of the mitochondrial membrane, resulting in loss of Ψ_M, and the release of mitochondrial cytochrome c into the cytosol [66]. These events in turn lead to the activation of the caspase 9/caspase 3 pathway, and subsequent chromatin condensation and DNA fragmentation [67]. In our study, PL treatment of Y79 cells resulted in the loss of Ψ_M, as evident by either the reduction or absence of red fluorescence in treated cells compared with untreated cells, following staining with JC-10 dye (Fig. 3). Additionally, PL-induced loss of Ψ_M was associated with significantly higher levels of caspase3/7 positive cells (Fig. 4) following staining with a caspase 3/7-specific dye. These results suggested that PL-induced apoptosis in metastatic RB likely involves the loss of Ψ_M and caspase 3/7 activation, which are associated with the mitochondrial-mediated intrinsic cell death pathway. These events remained insignificant in cells treated with similar doses (0, 5, and 10 μM) of either ETOP, CBP, or VINC. In contrast to our study, a recent study showed that PL-induced cell death in RB cells proceeds via cellular accumulation of ROS and caspase-3 independent cell death as evidenced by the presence of a cleaved caspase-3 band in staurosporine-treated cells and its absence in PL-treated cells [62]. It is not clear whether the caspase 3/7-dependent cell death in our study and the caspase-3-independent cell death reported by Allaman-Pillet et al. (2021) [62] are due to differences in caspase detection assays.

The data show PL facilitated reductions of *MYCN* mRNA transcripts in Y79 cells and their released EVs (Fig. 5A). Additionally, Y79 cells treated with PL-Y79-EVs resulted in decreased cell growth (Fig. 5B) and LCMS analysis detected PL in treated cells and released EV samples (Fig. 6). The data suggest that PL is internalized. It has been shown that PL is

internalized, undergoes intracellular hydrolysis, and binds to the intracellular protein GSTP1 [68]. Also, multiple studies demonstrate cell-based drug internalization and loading into EVs, to generate EV-drug carriers [69,70]. To the best of our knowledge, this is the first time a natural product is shown to reduce the pro-oncogenic contents of retinoblastoma EVs with the ability to reduce proliferation in recipient cells. The growth-inhibiting effects of the PL-Y79-EVs may be related to either 1) PL-induced downregulation of *MYCN* in Y79 EVs or 2) PL transferred to the treated cells via encapsulation or incorporation into EVs. Pharmacologic drug concentrations delivered in EVs, drug stability, and uptake in recipient cancer cells are well studied, demonstrating significant anti-cancer effects [71,72]. Either scenario seems logical. To further investigate the possible mechanism of the interaction between PL and MYCN, we performed a molecular docking of PL and Aurora A kinase, which is a crucial regulator of MYC function. As MYCN is considered undruggable due to its chemical structure, loss of function of Aurora A kinase can potentially lead to MYCN degradation. The docking results showed PL can be an ATP-competitive compound and block Aurora A from binding ATP at its ATP-binding pocket (Fig. 7). This will lead to an interruption of the protein-protein contact of Aurora A and MYCN, causing MYCN loss of protection and degradation. Interestingly, non-metastatic WERI-RB1-EVs incubated with WERI-RB1 cells can facilitate cell growth [73] angiogenesis and expression of pro-inflammatory cytokines [74], presumably as a consequence of pro-oncogenic cargo. In light of these studies, future work into the therapeutic efficacy of PL and other novel compounds that reduce the pro-oncogenic cargo of malignant EVs is warranted, since chemo-naïve and chemo-exposed cancer EVs harbor factors that can potentiate and promote metastasis [75] and chemotherapeutic resistance [76].

Supplementary Material

Refer to Web version on PubMed Central for supplementary material.

Acknowledgment

We thank Gail M. Seigel (University at Buffalo, the State University of New York) for her review of the manuscript. This work was made possible with grants from the National Institute of General Medical Sciences S.R. (5SC3GM113782) and the National Eye Institute S.R. (5R21EY026752-02).

Data availability

Data will be made available on request.

References

[1]. Aerts I, Lumbroso-Le Rouic L, Gauthier-Villars M, Brisse H, Doz F, Desjardins L, Retinoblastoma, Orphanet J. Rare Dis 1 (2006) 31. [PubMed: 16934146]

[2]. Berry JL, Kogachi K, Murphree AL, Jubran R, Kim JW, A Review of Recurrent Retinoblastoma: Children's Hospital Los Angeles Classification and Treatment Guidelines, Int Ophthalmol. Clin 59 (2) (2019) 65–75. [PubMed: 30908280]

[3]. Dimaras H, Kimani K, Dimba EA, Gronsdahl P, White A, Chan HS, Gallie BL, Retinoblastoma, Lancet 379 (9824) (2012) 1436–1446. [PubMed: 22414599]

[4]. Leander C, Fu LC, Peña A, Howard SC, Rodriguez-Galindo C, Wilimas JA, Ribeiro RC, Haik B, Impact of an education program on late diagnosis of retinoblastoma in Honduras, Pediatr. Blood Cancer 49 (6) (2007) 817–819. [PubMed: 17009236]

[5]. Fabius AWM, van Hoefen Wijsard M, van Leeuwen FE, Moll AC, Subsequent malignant neoplasms in retinoblastoma survivors, Cancers (Basel) 13 (6) (2021).

[6]. Dimaras H, Corson TW, Cobrinik D, White A, Zhao J, Munier FL, Abramson DH, Shields CL, Chantada GL, Njuguna F, Gallie BL, Retinoblastoma, Nat. Rev. Dis. Prim 1 (2015) 15021.

[7]. Hu H, Zhang W, Wang Y, Huang D, Shi J, Li B, Zhang Y, Zhou Y, Characterization, treatment and prognosis of retinoblastoma with central nervous system metastasis, BMC Ophthalmol. 18 (1) (2018) 107. [PubMed: 29685116]

[8]. Cozza R, De Ioris MA, Ilari I, Devito R, Fidani P, De Sio L, Demelas F, Romanzo A, Donfrancesco A, Metastatic retinoblastoma: single institution experience over two decades, Br. J. Ophthalmol 93 (9) (2009) 1163–1166. [PubMed: 19556217]

[9]. Gündüz AK, Mirzayev I, Temel E, Ünal E, Taçyıldız N, Dinçaslan H, Köse SK, Özalp Ateş FS, Işık MU, A 20-year audit of retinoblastoma treatment outcomes, Eye (Lond.) 34 (10) (2020) 1916–1924. [PubMed: 32376976]

[10]. Gündüz K, Müftüoglu O, Günalp I, Unal E, Taçyildiz N, Metastatic retinoblastoma clinical features, treatment, and prognosis, Ophthalmology 113 (9) (2006) 1558–1566. [PubMed: 16828510]

[11]. Finger PT, Harbour JW, Karcioglu ZA, Risk factors for metastasis in retinoblastoma, Surv. Ophthalmol 47 (1) (2002) 1–16. [PubMed: 11801265]

[12]. Choucair ML, Brisse HJ, Fréneaux P, Desjardins L, Dorfmüller G, Puget S, Dendale R, Chevrier M, Doz F, Lumbroso-Le Rouic L, Aerts I, Management of advanced uni- or bilateral retinoblastoma with macroscopic optic nerve invasion, Pedia Blood Cancer 67 (1) (2020), e27998.

[13]. Honavar SG, Singh AD, Management of advanced retinoblastoma, Ophthalmol. Clin. North Am 18 (1) (2005) 65–73 (viii). [PubMed: 15763192]

[14]. Errico A, Cancer therapy: retinoblastoma–chemotherapy increases the risk of secondary cancer, Nat. Rev. Clin. Oncol 11 (11) (2014) 623.

[15]. Shukla S, Srivastava A, Kumar S, Singh U, Goswami S, Chawla B, Bajaj MS, Kashyap S, Kaur J, Expression of multidrug resistance proteins in retinoblastoma, Int J. Ophthalmol 10 (11) (2017) 1655–1661. [PubMed: 29181307]

[16]. Talib WH, Alsayed AR, Barakat M, Abu-Taha MI, Mahmod AI, Targeting drug chemo-resistance in cancer using natural products, Biomedicines 9 (10) (2021).

[17]. Sarwar MS, Zhang HJ, Tsang SW, Perspectives of plant natural products in inhibition of cancer invasion and metastasis by regulating multiple signaling pathways, Curr. Med Chem 25 (38) (2018) 5057–5087. [PubMed: 28925869]

[18]. Galardi A, Colletti M, Lavarello C, Di Paolo V, Mascio P, Russo I, Cozza R, Romanzo A, Valente P, De Vito R, Pascucci L, Peinado H, Carcaboso AM, Petretto A, Locatelli F, Di Giannatale A, Proteomic profiling of retinoblastoma-derived exosomes reveals potential biomarkers of vitreous seeding, Cancers (Basel) 12 (6) (2020).

[19]. Keklikoglou I, Cianciaruso C, Güç E, Squadrito ML, Spring LM, Tazzyman S, Lambein L, Poissonnier A, Ferraro GB, Baer C, Cassará A, Guichard A, Iruela-Arispe ML, Lewis CE, Coussens LM, Bardia A, Jain RK, Pollard JW, De Palma M, Chemotherapy elicits pro-metastatic extracellular vesicles in breast cancer models, Nat. Cell Biol 21 (2) (2019) 190–202. [PubMed: 30598531]

[20]. He F, Li L, Fan R, Wang X, Chen X, Xu Y, Extracellular vesicles: an emerging regenerative treatment for oral disease, Front. Cell Dev. Biol 9 (2021).

[21]. Tai YL, Chu PY, Lee BH, Chen KC, Yang CY, Kuo WH, Shen TL, Basics and applications of tumor-derived extracellular vesicles, J. Biomed. Sci 26 (1) (2019) 35. [PubMed: 31078138]

[22]. Ab Razak NS, Ab Mutalib NS, Mohtar MA, Abu N, Impact of chemotherapy on extracellular vesicles: understanding the chemo-EVs, Front Oncol. 9 (2019) 1113. [PubMed: 31803605]

[23]. Fontana F, Carollo E, Melling GE, Carter D, Extracellular vesicles: emerging modulators of cancer drug resistance, Cancers (Basel) 13 (4) (2021).

[24]. Kogure A, Yoshioka Y, Ochiya T, Extracellular vesicles in cancer metastasis: potential as therapeutic targets and materials, Int J. Mol. Sci 21 (12) (2020).

[25]. Zhu P, Qian J, Xu Z, Meng C, Zhu W, Ran F, Zhang W, Zhang Y, Ling Y, Overview of piperlongumine analogues and their therapeutic potential, Eur. J. Med. Chem 220 (2021), 113471.

[26]. Tripathi SK, Biswal BK, Piperlongumine, a potent anticancer phytotherapeutic: Perspectives on contemporary status and future possibilities as an anticancer agent, Pharm. Res 156 (2020), 104772.

[27]. Kung FP, Lim YP, Chao WY, Zhang YS, Yu HI, Tai TS, Lu CH, Chen SH, Li YZ, Zhao PW, Yen YP, Lee YR, Piperlongumine, a Potent Anticancer Phytotherapeutic, Induces Cell Cycle Arrest and Apoptosis In Vitro and In Vivo through the ROS/Akt Pathway in Human Thyroid Cancer Cells, Cancers (Basel) 13 (17) (2021).

[28]. Liu D, Qiu XY, Wu X, Hu DX, Li CY, Yu SB, Pan F, Chen XQ, Piperlongumine suppresses bladder cancer invasion via inhibiting epithelial mesenchymal transition and F-actin reorganization, Biochem Biophys. Res Commun 494 (1–2) (2017) 165–172. [PubMed: 29037814]

[29]. Adams DJ, Dai M, Pellegrino G, Wagner BK, Stern AM, Shamji AF, Schreiber SL, Synthesis, cellular evaluation, and mechanism of action of piperlongumine analogs, Proc. Natl. Acad. Sci. USA 109 (38) (2012) 15115–15120.

[30]. Roh JL, Kim EH, Park JY, Kim JW, Kwon M, Lee BH, Piperlongumine selectively kills cancer cells and increases cisplatin antitumor activity in head and neck cancer, Oncotarget 5 (19) (2014) 9227–9238. [PubMed: 25193861]

[31]. Piska K, Gunia-Krzyżak A, Koczurkiewicz P, Wójcik-Pszczoła K, Pękala E, Piperlongumine (piplartine) as a lead compound for anticancer agents - Synthesis and properties of analogues: A mini-review, Eur. J. Med Chem 156 (2018) 13–20. [PubMed: 30006159]

[32]. Wu N, Jia D, Bates B, Basom R, Eberhart CG, MacPherson D, A mouse model of MYCN-driven retinoblastoma reveals MYCN-independent tumor reemergence, J. Clin. Invest 127 (3) (2017) 888–898. [PubMed: 28165337]

[33]. Gustafson WC, Meyerowitz JG, Nekritz EA, Chen J, Benes C, Charron E, Simonds EF, Seeger R, Matthay KK, Hertz NT, Eilers M, Shokat KM, Weiss WA, Drugging MYCN through an allosteric transition in Aurora kinase A, Cancer Cell 26 (3) (2014) 414–427. [PubMed: 25175806]

[34]. Richards MW, Burgess SG, Poon E, Carstensen A, Eilers M, Chesler L, Bayliss R, Structural basis of N-Myc binding by Aurora-A and its destabilization by kinase inhibitors, Proc. Natl. Acad. Sci. USA 113 (48) (2016) 13726–13731.

[35]. Gharbaran R, Shi C, Onwumere O, Redenti S, Plumbagin Induces Cytotoxicity via Loss of Mitochondrial Membrane Potential and Caspase Activation in Metastatic Retinoblastoma, Anticancer Res 41 (10) (2021) 4725–4732. [PubMed: 34593421]

[36]. Gharbaran R, Shang E, Onwumere O, Codrington N, Sarpong ED, Redenti S, Luteolin Induces Cytotoxicity in Mix Cellularity Classical Hodgkin's Lymphoma via Caspase Activated-cell Death, Anticancer Res 40 (9) (2020) 4907–4912. [PubMed: 32878778]

[37]. Comfort N, Cai K, Bloomquist TR, Strait MD, Jr Ferrante AW AA Baccarelli, Nanoparticle Tracking Analysis for the Quantification and Size Determination of Extracellular Vesicles, J. Vis. Exp (169) (2021).

[38]. Gharbaran R, Onwumere O, Codrington N, Somenarain L, Redenti S, Immunohistochemical localization of prolactin receptor (PRLR) to Hodgkin's and Reed-Sternberg cells of Hodgkin's lymphoma, Acta Histochem 123 (1) (2021), 151657.

[39]. Diebold M, Schönemann L, Eilers M, Sotriffer C, Schindelin H, Crystal structure of a covalently linked Aurora-A-MYCN complex, Acta Crystallogr D. Struct. Biol 79 (Pt 1) (2023) 1–9. [PubMed: 36601802]

[40]. Pettersen EF, Goddard TD, Huang CC, Couch GS, Greenblatt DM, Meng EC, Ferrin TE, UCSF Chimera–a visualization system for exploratory research and analysis, J. Comput. Chem 25 (13) (2004) 1605–1612. [PubMed: 15264254]

[41]. Delaney LM, Farias N, Ghassemi Rad J, Fernando W, Annan H, Hoskin DW, The natural alkaloid piperlongumine inhibits metastatic activity and epithelial-to-mesenchymal transition of

triple-negative mammary carcinoma cells, Nutr. Cancer 73 (11–12) (2021) 2397–2410. [PubMed: 33019824]

[42]. Ntagwabira F, Trujillo M, McElroy T, Brown T, Simmons P, Sykes D, Allen AR, Piperlongumine as a Neuro-Protectant in Chemotherapy Induced Cognitive Impairment, Int J. Mol. Sci 23 (4) (2022).

[43]. Kim N, Do J, Bae JS, Jin HK, Kim JH, Inn KS, Oh MS, Lee JK, Piperlongumine inhibits neuroinflammation via regulating NF-kappaB signaling pathways in lipopolysaccharide-stimulated BV2 microglia cells, J. Pharm. Sci 137 (2) (2018) 195–201.

[44]. Gottlieb E, Armour SM, Harris MH, Thompson CB, Mitochondrial membrane potential regulates matrix configuration and cytochrome c release during apoptosis, Cell Death Differ. 10 (6) (2003) 709–717. [PubMed: 12761579]

[45]. McIlwain DR, Berger T, Mak TW, Caspase functions in cell death and disease, Cold Spring Harb. Perspect. Biol 5 (4) (2013), a008656.

[46]. Kaufmann SH, Earnshaw WC, Induction of apoptosis by cancer chemotherapy, Exp. Cell Res 256 (1) (2000) 42–49. [PubMed: 10739650]

[47]. Madhavan J, Mitra M, Mallikarjuna K, Pranav O, Srinivasan R, Nagpal A, Venkatesan P, Kumaramanickavel G, KIF14 and E2F3 mRNA expression in human retinoblastoma and its phenotype association, Mol. Vis 15 (2009) 235–240. [PubMed: 19190782]

[48]. McEvoy J, Ulyanov A, Brennan R, Wu G, Pounds S, Zhang J, Dyer MA, Analysis of MDM2 and MDM4 single nucleotide polymorphisms, mRNA splicing and protein expression in retinoblastoma, PLoS One 7 (8) (2012), e42739.

[49]. Kalluri R, LeBleu VS, The biology, function, and biomedical applications of exosomes, Science 367 (6478) (2020).

[50]. Song H, Liu B, Dong B, Xu J, Zhou H, Na S, Liu Y, Pan Y, Chen F, Li L, Wang J, Exosome-Based Delivery of Natural Products in Cancer Therapy, Front Cell Dev. Biol 9 (2021), 650426.

[51]. Zugbi S, Ganiewich D, Bhattacharyya A, Aschero R, Ottaviani D, Sampor C, Cafferata EG, Mena M, Sgroi M, Winter U, Lamas G, Suñol M, Daroqui M, Baialardo E, Salas B, Das A, Fandiño A, Francis JH, Lubieniecki F, Lavarino C, Garippa R, Podhajcer OL, Abramson DH, Radvanyi F, Chantada G, Llera AS, Schaiquevich P, Clinical, Genomic, and Pharmacological Study of MYCN-Amplified RB1 Wild-Type Metastatic Retinoblastoma, Cancers (Basel) 12 (9) (2020).

[52]. Brabec V, Kasparkova J, Modifications of DNA by platinum complexes. Relation to resistance of tumors to platinum antitumor drugs, Drug Resist Updat 8 (3) (2005) 131–146. [PubMed: 15894512]

[53]. Zhou J, Kang Y, Chen L, Wang H, Liu J, Zeng S, Yu L, The drug-resistance mechanisms of five platinum-based antitumor agents, Front Pharm. 11 (2020) 343.

[54]. Kothari A, Hittelman WN, Chambers TC, Cell cycle-dependent mechanisms underlie vincristine-induced death of primary acute lymphoblastic leukemia cells, Cancer Res 76 (12) (2016) 3553–3561. [PubMed: 27197148]

[55]. Starobova H, Vetter I, Pathophysiology of chemotherapy-induced peripheral neuropathy, Front Mol. Neurosci 10 (2017) 174. [PubMed: 28620280]

[56]. Rodriguez-Galindo C, Wilson MW, Haik BG, Merchant TE, Billups CA, Shah N, Cain A, Langston J, Lipson M, Kun LE, Pratt CB, Treatment of intraocular retinoblastoma with vincristine and carboplatin, J. Clin. Oncol 21 (10) (2003) 2019–2025. [PubMed: 12743157]

[57]. King BA, Sahr N, Sykes A, Wilson MW, Brennan RC, Chemoreduction with topotecan and vincristine: Quantifying tumor response in bilateral retinoblastoma patients, Pedia Blood Cancer 68 (4) (2021), e28882.

[58]. Jin X, Liu K, Jiao B, Wang X, Huang S, Ren W, Zhao K, Vincristine promotes migration and invasion of colorectal cancer HCT116 cells through RhoA/ROCK/Myosin light chain pathway, Cell Mol. Biol. (Noisy-Le. -Gd.) 62 (12) (2016) 91–96.

[59]. van de Velde ME, Kaspers GL, Abbink F, Wilhelm AJ, Ket J, van den Berg MH, Vincristine-induced peripheral neuropathy in children with cancer: A systematic review, Crit. Rev. Oncol. Hematol 114 (2017) 114–130. [PubMed: 28477739]

[60]. Rezonja R, Knez L, Cufer T, Mrhar A, Oral treatment with etoposide in small cell lung cancer - dilemmas and solutions, Radio. Oncol 47 (1) (2013) 1–13.

[61]. Maria Fareed Siddiqui MMASS, Biochemical Mechanisms of Etoposide; Upshot of Cell Death, Int. J. Pharm. Sci. Res 6 (12) (2015) 4920–4939.

[62]. Allaman-Pillet N, Schorderet DF, Piperlongumine promotes death of retinoblastoma cancer cells, Oncotarget 12 (9) (2021) 907–916. [PubMed: 33953844]

[63]. Jeong CH, Ryu H, Kim DH, Cheng WN, Yoon JE, Kang S, Han SG, Piperlongumine Induces Cell Cycle Arrest via Reactive Oxygen Species Accumulation and IKKbeta Suppression in Human Breast Cancer Cells, Antioxid. (Basel) 8 (11) (2019).

[64]. Zhu X, Xue L, Yao Y, Wang K, Tan C, Zhuang M, Zhou F, Zhu L, The FoxM1-ABCC4 axis mediates carboplatin resistance in human retinoblastoma Y-79 cells, Acta Biochim Biophys. Sin. (Shanghai) 50 (9) (2018) 914–920. [PubMed: 30060118]

[65]. Winter E, Chiaradia LD, Silva AH, Nunes RJ, Yunes RA, Creczynski-Pasa TB, Involvement of extrinsic and intrinsic apoptotic pathways together with endoplasmic reticulum stress in cell death induced by naphthylchalcones in a leukemic cell line: advantages of multi-target action, Toxicol. Vitr 28 (5) (2014) 769–777.

[66]. Ott M, Robertson JD, Gogvadze V, Zhivotovsky B, Orrenius S, Cytochrome c release from mitochondria proceeds by a two-step process, Proc. Natl. Acad. Sci. USA 99 (3) (2002) 1259–1263. [PubMed: 11818574]

[67]. Madesh M, Hajnoczky G, VDAC-dependent permeabilization of the outer mitochondrial membrane by superoxide induces rapid and massive cytochrome c release, J. Cell Biol 155 (6) (2001) 1003–1015. [PubMed: 11739410]

[68]. Harshbarger W, Gondi S, Ficarro SB, Hunter J, Udayakumar D, Gurbani D, Singer WD, Liu Y, Li L, Marto JA, Westover KD, Structural and Biochemical Analyses Reveal the Mechanism of Glutathione S-Transferase Pi 1 Inhibition by the Anti-cancer Compound Piperlongumine, J. Biol. Chem 292 (1) (2017) 112–120. [PubMed: 27872191]

[69]. Herrmann IK, Wood MJA, Fuhrmann G, Extracellular vesicles as a next-generation drug delivery platform, Nat. Nanotechnol 16 (7) (2021) 748–759. [PubMed: 34211166]

[70]. Al-Jipouri A, Almurisi SH, Al-Japairai K, Bakar LM, Doolaanea AA, Liposomes or extracellular vesicles: a comprehensive comparison of both lipid bilayer vesicles for pulmonary drug delivery, Polym. (Basel) 15 (2) (2023).

[71]. Butreddy A, Kommineni N, Dudhipala N, Exosomes as naturally occurring vehicles for delivery of biopharmaceuticals: insights from drug delivery to clinical perspectives, Nanomater. (Basel) 11 (6) (2021).

[72]. Wang J, Yeung BZ, Cui M, Peer CJ, Lu Z, Figg WD, Guillaume Wientjes M, Woo S, Au JL, Exosome is a mechanism of intercellular drug transfer: Application of quantitative pharmacology, J. Control Release 268 (2017) 147–158. [PubMed: 29054369]

[73]. Chen S, Chen X, Qiu J, Chen P, Han X, Wu Y, Zhuang J, Yang M, Wu C, Wu N, Yang Y, Ge J, Yu K, Zhuang J, Exosomes derived from retinoblastoma cells enhance tumour deterioration by infiltrating the microenvironment, Oncol. Rep 45 (1) (2021) 278–290. [PubMed: 33416154]

[74]. Chen S, Chen X, Luo Q, Liu X, Wang X, Cui Z, He A, He S, Jiang Z, Wu N, Chen P, Yu K, Zhuang J, Retinoblastoma cell-derived exosomes promote angiogenesis of human vesicle endothelial cells through microRNA-92a-3p, Cell Death Dis. 12 (7) (2021) 695. [PubMed: 34257272]

[75]. Bao Q, Huang Q, Chen Y, Wang Q, Sang R, Wang L, Xie Y, Chen W, Tumor-derived extracellular vesicles regulate cancer progression in the tumor microenvironment, Front Mol. Biosci 8 (2021), 796385.

[76]. Maleki S, Jabalee J, Garnis C, The role of extracellular vesicles in mediating resistance to anticancer therapies, Int J. Mol. Sci 22 (8) (2021).

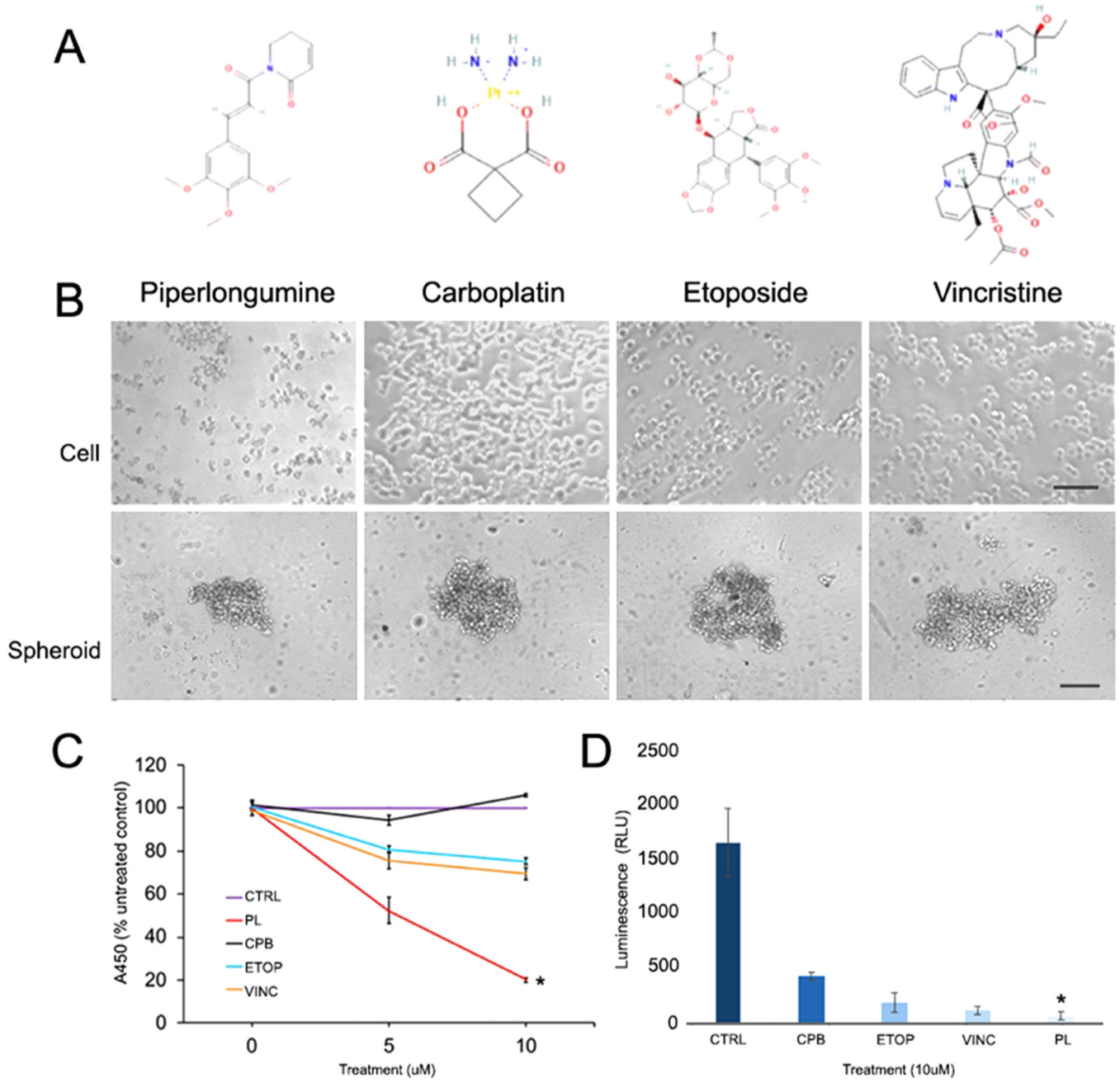

Fig. 1.

PL significantly reduces the viability of Y79 cells and spheroids compared to chemotherapeutic drugs. A) Chemical structures of PL, CBP, ETOP, and VINC. B) Phase contrast images comparing the morphology of cell and spheroids treated with (0, 5, and 10 μM) of each compound for 48 h. C) WST-1 cell proliferation assay shows PL induces a significant decrease in cell viability compared to chemotherapeutic drugs (One-way ANOVA, $p < 0.05$). D) CellTiter-Glo 3D spheroid viability assay also shows PL induces a significant decrease in cell viability compared to chemotherapeutic drugs (One-way

ANOVA, p = 0.0029, <0.05). PL, piperlongumine; CPB, carboplatin; ETOP, etoposide; VINC, vincristine. Cell scale = 50 μm, spheroid scale = 100 μm.

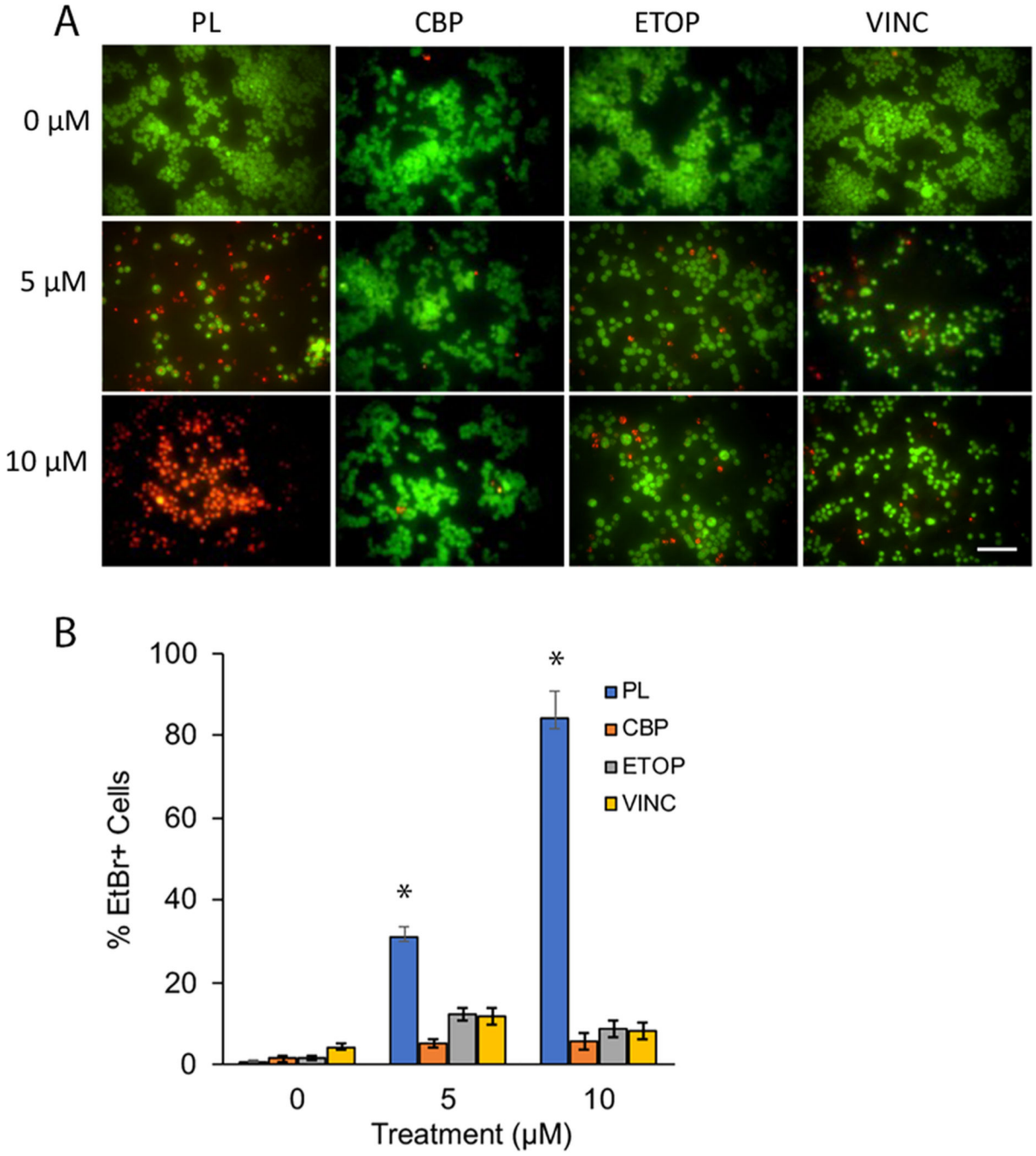

Fig. 2.

PL potently induces greater cell death compared to chemotherapeutic drugs in Y79 cells. A) Images qualitatively showing the effects of PL compared to CBP, ETOP, OR VINC on Y79 cells. B) PL resulted in statistically significant levels of cell death compared to chemotherapeutic drugs CBP, ETOP, and VINC (One-way ANOVA, $p < 0.05$). Y79 cells incubated overnight were treated with 0, 5, and 10 μM of each compound for 48 h then stained with AO-EtBr solution and imaged immediately.

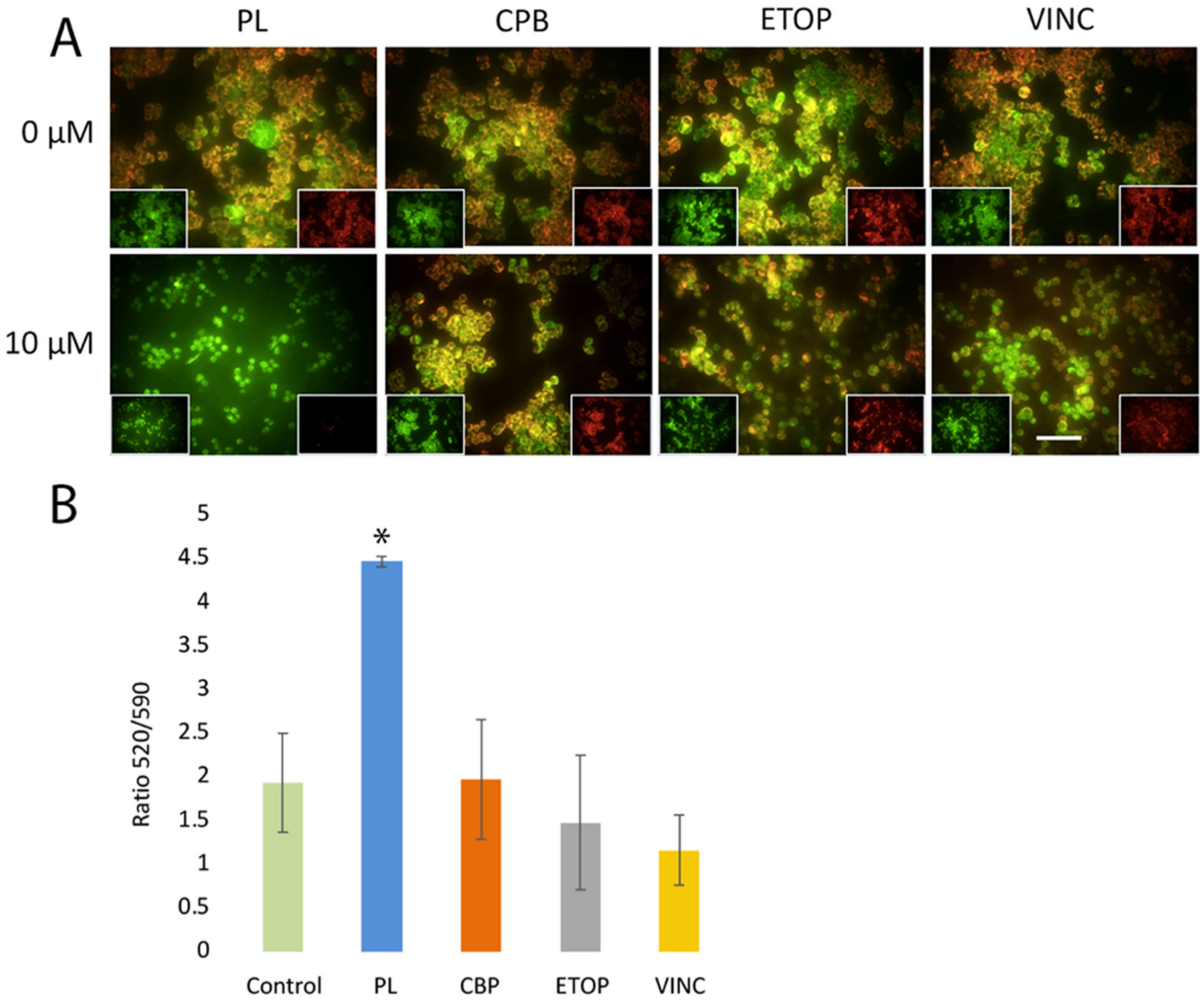

Fig. 3.

PL is associated with a significant loss of mitochondrial membrane potential. PL-treated Y79 cells showed significant depolarization of mitochondrial membrane potential compared to CBP, ETOP, or VINC treatments. A) Viable cells with mitochondria membrane potential (Ψ_M) maintained exhibit red fluorescence (590 nm) localized to the mitochondria matrix. In PL-treated cells, the mitochondrial matrix is significantly depolarized compared to the control (two-tailed t-test, $P < 0.0001$), leading to JC-10 diffusion out of mitochondria, and conversion to its monomeric form, leading to loss of red fluorescence and increased green (520 nm) fluorescence. B) The ratio of 520/590 is significantly increased for 10 μM PL treated cells compared to control or 10 μM of either CBP, ETOP, or VINC. Scale bar = 50 μm.

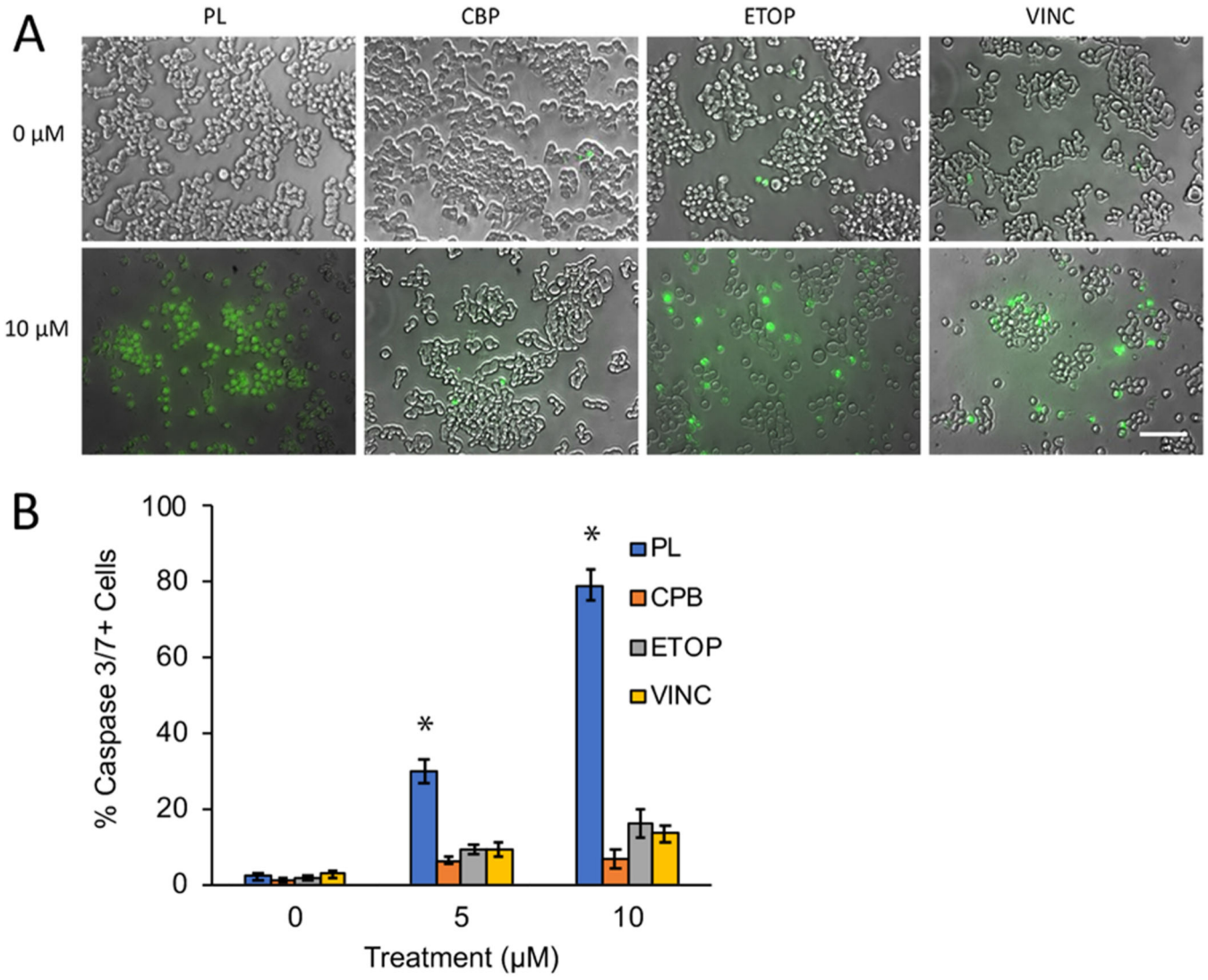

Fig. 4.

PL treatment was associated with significantly greater levels of caspase 3/7 activity. A) Representative images of Y79 cells treated with 10 μM of PL, CBP, ETOP, or VINC. Caspase3/7 + cells stained green, indicating caspase activation. B) PL treatment resulted in a significantly higher proportion of caspase3/7 (green) positive cells, compared to either CBP, ETOP, or VINC at 10 μm (One-way ANOVA, $p < 0.05$).

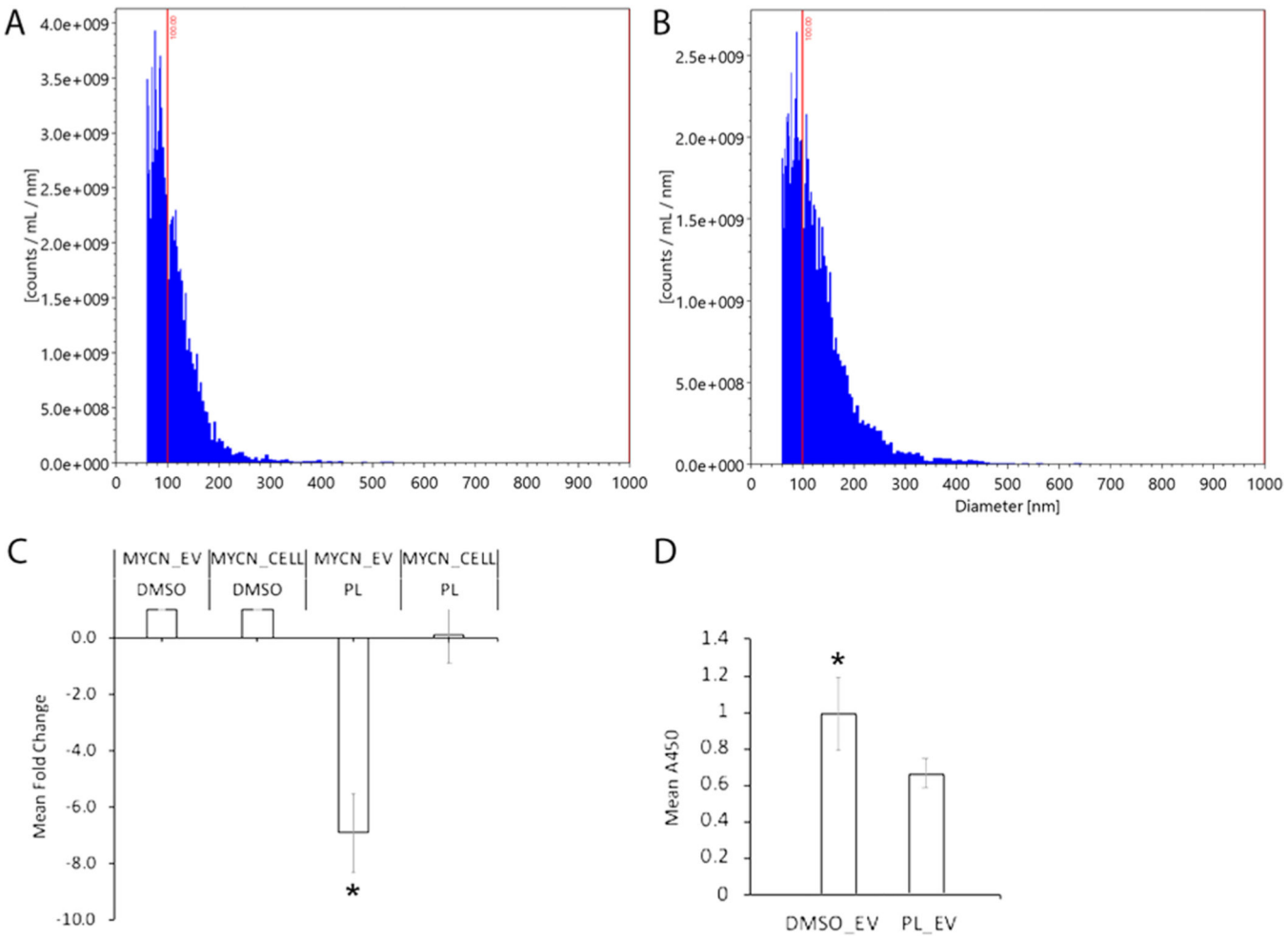

Fig. 5.

PL downregulates MYCN contained in EVs and reduces the growth of Y79 cells. ViewSizer 3000 nanoparticle particle analysis allowed for the characterization of Y79 EV diameters and release rate. A) The average diameter for control Y79 EVs was 148 nm ± 59 nm with a concentration of 1.1E+ 11 particles/ml. B) PL-treated experimental Y79-EVs exhibited an average diameter of 164 nm ± 68 nm at a concentration of 1.3E+ 11 particles/ml. C) Following PL treatment, qPCR revealed a significant downregulation of MYCN transcripts in Y79 EVs (MYCN_EV PL) ($p < 0.05$). MYCN downregulation was observed in cells (MYCN_CELL PL) ($p < 0.05$). D) Untreated Y79 cells treated with EVs from PL-treated Y79 cells (PL_ EVs) exhibited a significant reduction in cell growth compared to control EVs from Y79 cells cultured in DMSO, (DMSO_EVs) (One-way ANOVA, $p < 0.05$).

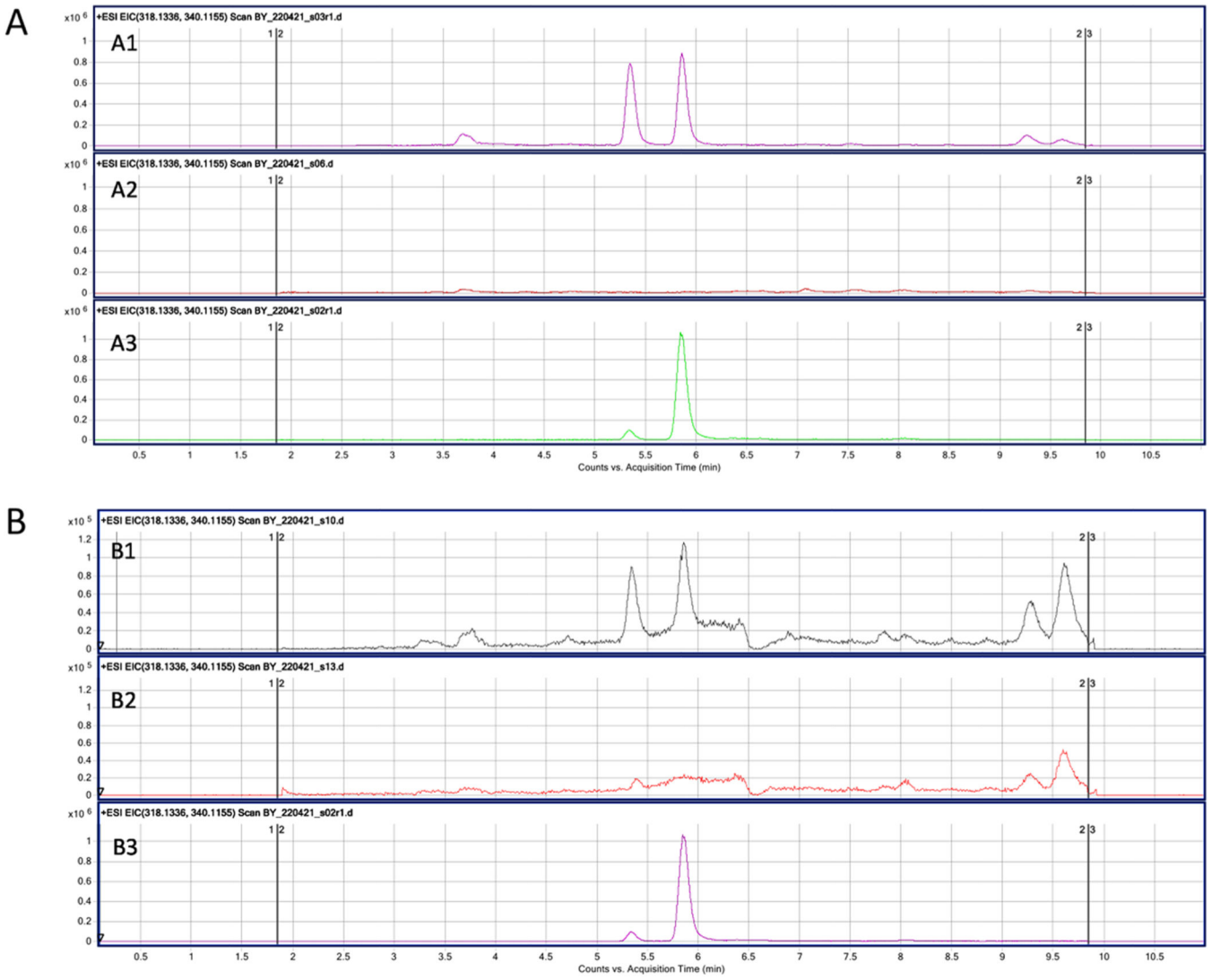

Fig. 6.

UPLC-MS analysis of PL treated Y79 cell and EV extract. PL was suspended in 100 μL of water/acetonitrile; 5 μL was injected. The chromatogram of the PL standard shows the peak at a retention time of 5.86 (A3, Fig. B3). Both the PL-treated Y79 cell extract (A1) and EV released from the PL-treated cells (B1) show peaks at the same retention time, which are not present in the untreated cells (A2) and EVs (B2) samples, which aligns with peaks in PL cell and EV experimental samples. PL was detected in Y79 cell samples with an estimated concentration of 0.310pM and EV samples with an estimated concentration of 0.026pM. PL standard for cells (A3) and EVs (B3).

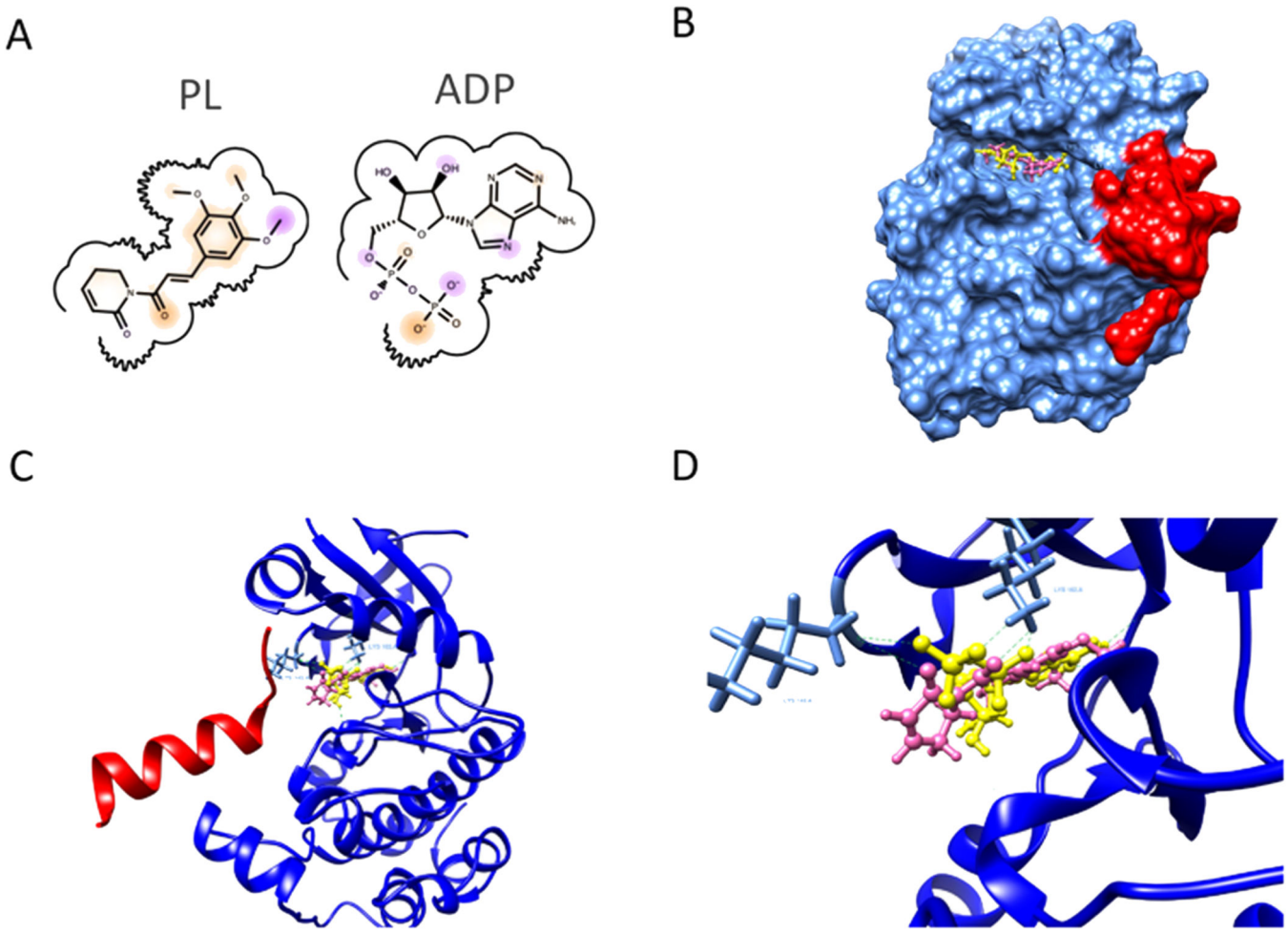

Fig. 7.

Molecular docking of PL and Aurora A. A. Chemical structures of ADP and PL. B. Surface representation of Aurora A(blue) MYCN(red) complex and PL(pink) in ATP binding pocket. C. Docking poses showing the interaction between PL(pink), ADP(yellow), and Aurora A (blue)/MYCN(red) complex(PDB: 7ZTL). D. Detailed interaction at the ATP-binding pocket. Green dotted lines show possible hydrogen binds formation between Aurora A protein and PL or ADP at residue LYS143A and LYS162A.